Eur. Phys. J. A (2023) 59:82
https://doi.org/10.1140/epja/s10050-023-00993-x

THE EUROPEAN PHYSICAL JOURNAL A

Regular Article - Experimental Physics

Gamma-ray energies and intensities observed in decay chain ^{83}Rb/^{83m}Kr/^{83}Kr

M. Šefčík[1,a], **D. Vénos**[1], **O. Lebeda**[1], **C. Noll**[2], **J. Ráliš**[1]

[1] Nuclear Physics Institute of the Czech Academy of Sciences, Řež 130 25068, Czech Republic
[2] Helmholtz Institut für Strahlen- und Kernphysik, Universität Bonn (HISKP), Nussallee 14-16, Bonn 53115, Germany

Received: 10 February 2023 / Accepted: 29 March 2023 / Published online: 20 April 2023

Communicated by Navin Alahari

Abstract Radioactive sources of the monoenergetic low-energy conversion electrons from the decay of isomeric ^{83m}Kr are frequently used in the systematic measurements, particularly in the neutrino mass and dark matter experiments. For this purpose, the isomer is obtained by the decay of its parent radionuclide ^{83}Rb. In order to get more precise data on the gamma-rays occuring in the ^{83}Rb/^{83m}Kr chain, we re-measured the relevant gamma-ray spectra, because the previous measurement took place in 1976. The obtained intensities are in fair agreement with the previous measurement. We have, however, improved the uncertainties by a factor of 4.3, identified a new gamma transition and determined more precisely energies of weaker gamma transitions.

1 Introduction

^{83m}Kr is formed by the decay of ^{83}Rb (half-life 86.2 ± 1 day) via electron capture (EC). Approximately three quarters of ^{83}Rb decays result in the isomer ^{83m}Kr ($T_{1/2} = 1.83$ h). It further decays by the cascade of the 9.4 and 32.2 keV nuclear transitions to the ^{83}Kr ground state. Due to the low energy and high multipolarity (E3 for the 32.2 keV transition) of the transitions, the intense conversion electrons are emitted. These monoenergetic electrons are extensively used for the calibration and systematic measurements in the neutrino mass experiments (KATRIN, Project 8) [1,2], dark matter experiments [3,4] and also in the ALICE and COHERENT projects [5,6]. In all these experiments the ^{83}Rb is deposited into a suitable substrate, from which the daughter ^{83m}Kr emanates. The last primary data on the gamma-ray intensities in ^{83}Rb decay were published several decades ago, see [7,8]. The recent compilation and evaluation of the relevant data are available in the Nuclear Data Sheets (NDS) [9]. In the frame of our development of the ^{83m}Kr sources for the neutrino project KATRIN, see [10,11], we also re-measured the gamma-ray spectra present in the ^{83}Rb decay.

2 Measurement

Rubidium isotopes were produced at the NPI CAS Řež cyclotron TR-24 in the reactions ^{nat}Kr(p,xn)^{83,84,86}Rb using a pressurized gas target. The target filled with pure natural krypton at pressure of 10 bar was bombarded with 23 MeV protons at 45 μA beam current. The production yields of ^{83}Rb, ^{84}Rb and ^{86}Rb isotopes amounted to approximately 150, 90 and 25 MBq per one hour of the bombardment. The activity was extracted from the irradiated target by its thorough washout by water. Resulting aqueous solution was concentrated by evaporation and used for the activity deposition into the tungsten furnaces. The furnaces were then delivered to HISKP, where the gamma sources were prepared by the implantation of the separated ^{83}Rb ions with energy of 8 keV into the 0.5 mm thick Highly Oriented Pyrolytic Graphite (HOPG) substrate. The ^{83}Rb activity in the sources was about 3 MBq. Another type of the source was prepared in the NPI by evaporation of the rubidium isotopes solution pipetted on the 2.5 μm thick mylar foil. For the spectra acquisition, two gamma-ray detectors were used: an Ortec HPGe detector with the relative efficiency of 24.1 % and the energy resolution of 1.9 keV at 1.33 MeV, and a low energy Canberra SiLi detector with the diameter and thickness of 10.1 and 5 mm, respectively, and the energy resolution of 180 eV at 5.9 keV. Both detectors were equipped with a beryllium window. The Canberra spectrometric chains were used for the signal processing: amplifier 2025 and multichannel analyzer Multiport II controlled with the Genie 2000 software. The ADC gain conversion was set at 8192 and 4096 channels for the HPGe and SiLi detector, respectively. The distance

[a] e-mail: sefcik@ujf.cas.cz (corresponding author)

between the detector Be window and the measured source was set to 240 and 45.7 mm for the HPGe and SiLi detector, respectively. In order to reduce the sum peaks of the intense ^{83}Rb gamma-rays with the energies of 520.4, 529.6 and 552.5 keV with the accompanying strong krypton K X-rays, the nickel foil of 20 μm thickness was applied on the HPGe Be window. The measured spectra were analysed with the DEIMOS32 software [12].

The energy and detection efficiency calibrations were performed using the standards of ^{55}Fe (EFX type), and ^{133}Ba, ^{152}Eu and ^{241}Am (all three EG3 type) provided by the Czech Metrology Institute (CMI). Since the calibration sources are encapsulated in the polymethylmethacrylate (PMMA) and polyethylene, the attenuation of the gamma-rays in these materials was also measured to take it into account in the efficiency calibration. The efficiencies, measured with each standard separately, were normalized using the certificated activities supplied by CMI and the corresponding half-lives. The dependence of the efficiency $\varepsilon(E)$ on the gamma-ray energy E was χ^2-fitted using the 5 parameter formula $\varepsilon(E) = \sum p_i[ln(E+p_4)]^i$ where $i = 0, 1, 2, 3$. The efficiency of the HPGe detector was calibrated in the low (26–244 keV) and high (244–778 keV) energy regions with the uncertainties of 2.5 and 0.9 %, respectively. In the case of the SiLi detector, the efficiency was determined with the uncertainty of 2 % in the energy region of 5.9–33 keV. The normalized χ^2 was close to 1.

In Figs. 1 and 2, examples of the ^{83}Rb gamma-ray spectra measured with the HPGe and SiLi detectors, respectively, are displayed. Contamination lines present in the measured spectra were mainly caused by the terrestrial background. Terrestrial background lines were identified by measuring the spectra without the ^{83}Rb source. The other contaminations were induced by the ^{83}Rb source itself. In the case of the SiLi spectrum, the weak X-ray lines of Cr, Fe, Cu and Au elements (present in the detector material), were induced by the fluorescence effect, and the Si X-ray escape peak at 10.9 keV was visible. Moreover, the pile-up effect of the 9.4 keV line and Krypton 12.6 and 14.1 keV X-rays produced weak spectral peaks in the energy range of 22–27 keV. Finally, the effects of the detector dead-layer [13] and the Compton scattering [14] produced the line tailing apparent on the low energy side of the strong Krypton X-ray lines. The Pb X-rays were also present in the case of the HPGe spectra due to lead detector shielding. The measured gamma-ray energies and intensities are summarized in Table 1. The gamma-ray energies were determined with the HPGe detector in the special measurements of ^{83}Rb source together with the ^{152}Eu or ^{133}Ba standards, the gamma-rays of which were used for the calibration of the energy scale. The weak gamma transitions with the energies of 128.3 and 562.03 keV, respectively, were less distinct in the spectra acquired with the standards due to the additional Compton background. That is why the spectra

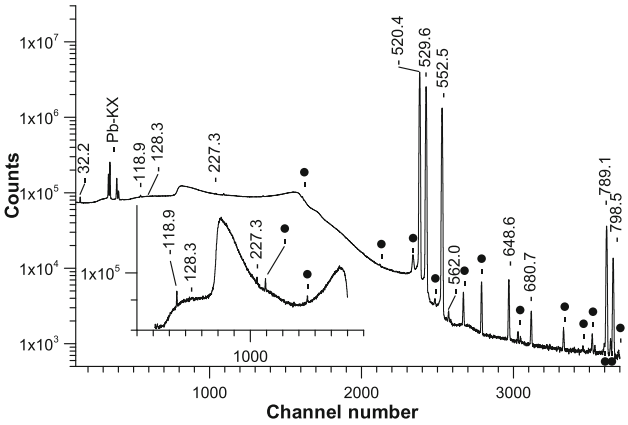

Fig. 1 Spectrum of ^{83}Rb acquired with the HPGe detector. The γ-lines which belong to the ^{83}Rb decay are marked by their energies in keV. The multiple lines denoted as Pb-KX are due to the fluorescence effect in the detector Pb shielding. The contamination lines are marked by black points

with the sole ^{83}Rb source were used in their evaluation. For the energy calibration, suitable gamma lines from the background and stronger ^{83}Rb lines, the energy of which was determined previously by us, were employed. Our energies of the three strongest gamma lines in the ^{83}Rb decay agree well with the very precise values in [9] which were adopted from [15]. The energies of the remaining lines are slightly lower (by 0.1–1.0 keV) and were obtained with better precision in comparison with those in [8,9]. We observed all gamma-rays presented in [9] except for the 237.19 keV for which the upper limit of its relative intensity of only 0.0011 was estimated. We are not able to observe it due to the presence of the intense 238.632(2) keV gamma line of ^{212}Pb [16] from the ^{232}Th decay chain. In contrast, we observed the 227.35(5) keV gamma line that is missing in [9]. The previous NDS review for A = 83 [17] listed this transition with the relative intensity of 0.03. The line was clearly visible in the spectra taken with our two different implanted sources. The half-life of this weak line was also determined to be of 90(+21, −12) days, which agrees well with the ^{83}Rb half-life of 86.2(1) days. This transition also fits very well into the decay scheme between the nuclear levels 798.5 and 571.1 keV, see Fig. 3.

After implantation of ^{83}Rb, the amount of the daughter ^{83m}Kr nuclei in HOPG substrate increases and within several ^{83m}Kr half-lives, the equilibrium is achieved. The amount of ^{83m}Kr starts then to decrease practically with the half-life of the parent ^{83}Rb. The possible emanation of the ^{83m}Kr out of the substrate may reduce the measured intensities of the 9.4 and 32.2 keV ^{83m}Kr gamma transitions (the decaying ^{83m}Kr nuclei find themselves outside the detection sensitive solid angle). Therefore we accomplished the measurement of the ^{83m}Kr retention in the implanted source. For this purpose, the HOPG substrate with the implanted source was placed

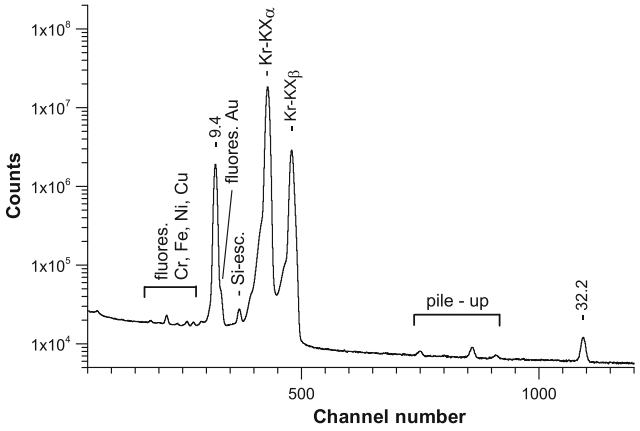

Fig. 2 The low energy spectrum of ^{83}Rb acquired with the SiLi detector. Besides the two gamma-rays resulting from the decay of its daughter ^{83m}Kr, the krypton K X-rays are present. The spectral lines caused by the fluorescence, escape and pile-up effects are also indicated

on the top of a closeable cylindrical chamber. The bottom part of the chamber was equipped with a thin PMMA window allowing the detection of the gamma-rays with the SiLi detector. The chamber design is further described in [19]. Using the 32.2 gamma-ray rates measured with the chamber closed and open at the fixed distance of the HOPG substrate from SiLi detector, the retention of ^{83m}Kr in the substrate was determined to be 0.974(19), thus, some emanation occurs.

The relative intensities of the 9.4 and 32.2 keV gamma transitions were corrected for the measured retention value. Our uncertainties of the gamma-ray intensities are on average smaller by a factor of 4.3 than previously published values. In our ^{83}Rb decay scheme (Fig. 3), the feedings of the ^{83}Kr levels by the electron capture and the log ft values are listed. The feeding was calculated as the normalized difference of the transition intensities de-exciting and feeding the given level. An assumption on the feeding of the Kr ground state at a level of 2.5 ± 2.5 % according to [9] was taken into account. The total intensity of the 32.2 keV transition, representing the number of ^{83m}Kr nuclei produced per 100 ^{83}Rb decays, is 76(3) %. In contrast to [9], our analysis demonstrated non-zero feeding of 4(3) % of the krypton isomeric state from the EC decay.

3 Conclusion

We have re-measured the gamma-ray spectra observed in the ^{83}Rb/^{83}Kr decay chain by means of HPGe and SiLi detectors. The values of the gamma-ray intensities are close to those in the previous paper [9]. Nevertheless, their uncertainties have been improved by a factor of 4.3 on average. The feeding of the ^{83}Kr levels from the EC decay with the relevant log ft values have also been determined. For the first time, we have observed the non-zero feeding of the iso-

Table 1 The measured ^{83}Rb gamma-ray energies and relative intensities related to the 520.4 keV transition (100 %). The total conversion coefficients and the transition intensities of the ^{83}Rb decays based on the level feeding (see Fig. 3) are also present. In the last two columns, the energies and intensities from [9] are listed for comparison

Energy E_γ (keV)	γ-ray relative intensity	Multipolarity **	Total conversion coefficient α_{tot}^{**}	Transition intensity (%)	Energy E_γ (keV) [9]	γ-ray relative intensity [9]
9.4057 (6)*	13.1 (6)	M1+E2	16.3 (2)	98 (4)	9.4057 (6)	13 (3)
32.1516 (5)*	0.090 (3)	E3	1950 (30)	76 (3)	32.1516 (5)	0.08 (1)
118.91 (5)	0.032 (2)	(M1+E2)	0.3 (2)	0.018 (3)	119.32 (9)	0.032 (5)
128.3 (1)	0.006 (2)	[M1+E2]	0.2 (2)	0.0030 (9)	128.6 (1)	0.0030 (5)
227.35 (5)	0.017 (2)	(E1)	0.0081 (1)	0.0073 (8)	–	–
–	–		–		237.19	< 0.0011
520.397 (2)	100.0 (9)	E2	0.00283 (4)	43.5 (4)	520.3991 (5)	100 (5)
529.591 (4)	65.1 (6)	(M1+E2)	0.00191 (3)	28.3 (3)	529.5945 (6)	66 (3)
552.547 (4)	35.5 (3)	(E1)	0.00076 (1)	15.4 (1)	552.5512 (7)	36 (2)
562.03 (6)	0.016 (1)	(M2)	0.00499 (7)	0.0071 (5)	562.17 (7)	0.019 (2)
648.58 (1)	0.197 (2)	E2	0.00150 (2)	0.0853 (9)	648.97 (5)	0.19 (1)
680.69 (3)	0.062 (1)	[E1]	0.00047 (1)	0.0269 (6)	681.18 (7)	0.07 (1)
789.105 (3)	1.51 (1)	(M1+E2)	0.00088 (1)	0.653 (6)	790.15 (4)	1.47 (4)
798.516 (5)	0.548 (5)	E2	0.00086 (1)	0.248 (2)	799.37 (5)	0.53 (2)

* The energies for the 9.4 and 32.2 transitions are adopted from [9]

** The total conversion coefficients were calculated with the software available in [18]. In the calculations, the transition multipolarities from [9] were used. For the 227.3 and 562.0 keV transitions, not indicated in the reference, the values of E1 and M2, respectively, were used as the most probable values

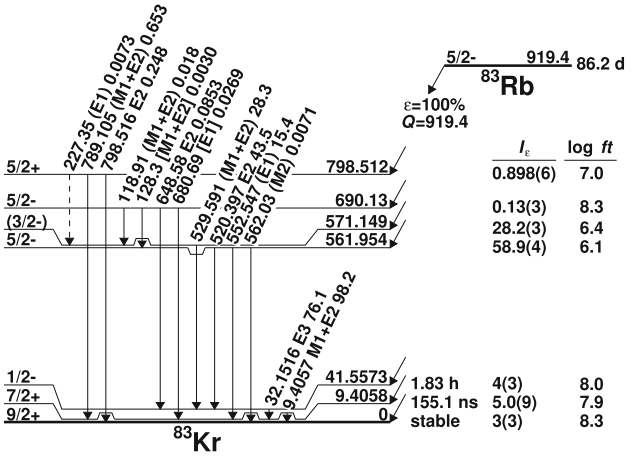

Fig. 3 Decay scheme of ^{83}Rb. The spin and parity assignment, half-lives and most multipolarities were adopted from [9]. The log ft values were calculated according to [20]

meric state at the level of 4 ± 3 %. Moreover, the 227.35 keV gamma transition has been measured and recommended to be introduced into the ^{83}Rb decay scheme. The gaseous ^{83m}Kr, whose monoenergetic electrons have widely been used for the systematic physical measurement, is produced in the 76(3) % of the ^{83}Rb decays.

Acknowledgements This work was supported by the Ministry of Education, Youth and Sport of the Czech Republic (projects LTT19005 and LM2015056) and the Czech Academy of Sciences.

Funding Information Open access publishing supported by the National Technical Library in Prague.

Data Availability Statement This manuscript has no associated data or the data will not be deposited. [Authors' comment: The relevant data is available from the authors upon reasonable request.]

References

1. KATRIN collaboration, Nat. Phys. **18**, (2022) 160–166
2. Project 8 collaboration, J. Phys. G: Nucl. Partic. **44**, (2017) 054004
3. W.X. Xiong, M.Y. Guan, C.G. Yang, P. Zhang, J.C. Liu, C. Guo, Y.T. Wei, Y.Y. Gan, Q. Zhao, J.J. Li, Radiat. Detect. Technol. Methods **4**, 147–152 (2020)
4. A.G. Singh, E.P. Bernard, A. Biekert, E.M. Boulton, S.B. Cahn, N. Destefano, B.N.V. Edwards, M. Gai, M. Horn, N. Larsen, Q. Riffard, B. Tennyson, V. Velan, C. Wahl, D.N. McKinsey, J. Instrum. **15**, P01023–P01023 (2020)
5. ALICE collaboration, Nucl. Instrum. Method A **881**, 88–127 (2018)
6. COHERENT collaboration, J. Instrum. **16**, P04002 (2021)
7. I. Dostrovsky, S. Katcoff, A.W. Stoenner, Phys. Rev. **136**, B44–B49 (1964)
8. S. Väisälä, G. Graeffe, J. Heinonen, A.A. Delucchi, R.A. Meyer, Phys. Rev. C **13**, 372–376 (1976)
9. E.A. McCutchan, Nucl. Data Sheets **125**, 201–394 (2015)
10. M. Suchopár, D. Vénos, O. Dragoun, O. Lebeda, M. Ryšavý, J. Sentkerestiová, A. Špalek, M. Slezák, K. Schlösser, M. Sturm, M. Arenz, C. Noll, poster at the 23rd Int. Conf. Neutrino Phys. Astrophys. (2018)
11. O. Lebeda, D. Vénos, J. Ráliš, M. Šefčík, O. Dragoun, poster at the 30th Int. Conf. Neutrino Phys. Astrophys. (2022)
12. J. Frána, J. Radioanal. Nucl. Chem. **257**, 583–587 (2003)
13. J.L. Campbell, A. Perujo, B.M. Millman, X-Ray Spectrom. **16**, 195–201 (1987)
14. J.L. Campbell, J.X. Wang, W.J. Teesdale, Nucl. Instrum. Method B **43**, 490–496 (1989)
15. T. Chang, S. Wang, H. Wang, B. Meng, Nucl. Instrum. Method A **325**, 196–204 (1993)
16. K. Auranen, E.A. McCutchan, Nucl. Data Sheets **168**, 117–267 (2020)
17. D.C. Kocher, Nucl. Data Sheets **15**, 169–201 (1975)
18. T. Kibédi, T.W. Burrows, M.B. Trzhaskovskaya, P.M. Davidson, C.W. Nestor, Nucl. Instrum. Method A **589**, 202–229 (2008)
19. D. Vénos, M. Slezák, O. Dragoun, A. Inoyatov, O. Lebeda, Z. Pulec, J. Sentkerestiová, A. Špalek, J. Instrum. **9**, P12010 (2014)
20. C. M. Lederer, V. S. Shirley, *Table of isotopes* (John Wiley & Sons, Inc., Hoboken, New Jersey, USA 1978) Appendix V, 19